Agora of Additive Manufacturing (2024) paper24003

JAMS

Agora of Additive Manufacturing

journal homepage: http://additive-manufacturing.or.jp/

Compressive strength of 3D-printed unidirectional carbon fiber/PA-6 composites: Effect of surface-layer printing using short carbon fiber/PA-6 composites

Ahmad Zuhair bin Zakaria[a], Akira Todoroki[b*], Masahito Ueda[c]

[a] Tokyo Institute of Technology, 2-12-1 Ookayama, Meguro, Tokyo, 1528550, Japan

[b] Graduate School of Tokyo Institute of Technology, 2-12-1 Ookayama, Meguro, Tokyo, 1528550, Japan

[c] Nihon University, 1-8-14 Kanda-Surugadai, Chiyoda, Tokyo, 1018308, Japan

ABSTRACT

The present study experimentally investigated the compressive strength of 3D-printed continuous carbon fiber composites. Two types of specimens were fabricated: type A was printed with the specimen thickness direction as the layup direction, and type B was printed with the specimen width direction as the layup direction. In previous research, these specimens were printed without surface layers (such as walls, floors, and roofs) using short carbon-fiber composite filaments, resulting in approximately 20% lower compressive strength compared with the Markforged datasheet. In this study, the specimens were printed with surface layers. The compressive strength showed results almost identical to those in the Markforged datasheet. To investigate the effect of the surface layers, the fiber waviness of the specimens was examined using X-ray computed tomography. The results indicated that the surface layers exhibited lesser waviness, leading to higher compressive strength.

Keywords: 3D printing, Composites, Compressive strength, waviness

1. Introduction

The typical compression failure mode of unidirectional carbon fiber-reinforced plastic (CFRP) is kink-band failure. This failure mode is caused by the local shear instability of the fiber and matrix microstructure when compressive stress is applied to the unidirectional CFRP, leading to fiber breakage within a narrow band region [(1–6)]. For kink-band failure under compressive loading, many researchers have reported that the initial waviness of fibers has a significant effect [(1–8)]. When a compressive load is applied to fibers with waviness, the waviness increases, and the matrix cannot withstand the shear deformation between the fibers, resulting in fiber breakage and kink-band failure. In traditional CFRP made by laminating prepregs, the waviness remains relatively stable. Consequently, the compressive strength can be reliably considered a material property.

Markforged has recently developed a 3D printer capable of printing continuous-fiber CFRP (cCFRP) [(9)]. Matsuzaki et al. developed a nozzle impregnation method to produce continuous-fiber composite materials [(10)]. Research papers have been published on the tensile tests of 3D-printed cCFRP [(11–13)]. Regarding the compressive strength of 3D-printed continuous fiber unidirectional CFRP, Iragi et al. conducted an American Standard for Testing and Materials (ASTM) D3410 unidirectional compression test and reported a compressive strength of *426* MPa [(14)]. In 3D printing, the waviness of cCFRP may vary due to printing conditions. This variation can result in the compressive strength no longer being consistent with the material's properties. This issue is rarely observed in CFRP produced by laminating prepregs.

* Corresponding author
Email: todoroki.a.aa@m.titech.ac.jp
Received 27 May 2024; Revised 24 July 2024; Accepted 26 July 2024
Available online 26 July 2024

Ahmad Zuhair et al. used a Markforged 3D printer to fabricate cCFRP specimens with only continuous fiber filaments, without surface layers such as walls, floors, and roofs, and conducted compression tests [15]. Two types of compression tests were performed: Type A, where the thickness direction of the specimen was the layup direction in the 3D printer, and Type B, where the width direction of the specimen was the layup direction. Compressive strengths of *347* MPa for a *2* mm thick type A specimen and *323* MPa for a *2* mm thick type B specimen were obtained. These strengths were significantly lower than the compressive strength of *420* MPa in the Markforged datasheet [16]. Additionally, the stress–strain diagram of type B differed from that of type A, with the measured stress–strain curves obtained from the front and back sides deviating from the initial state of the compression test. In 3D printing, the waviness of the material can vary. In the previous study done by Ahmad Zuhair et al. [17], the cCFRP were printed without surface layers, resulting in a lower compressive strength value compared to those in the Markforged datasheet. The absence of the surface layers may have increased the waviness of cCFRP. In this study, we will print cCFRP with a surface layer (wall path) and compare the results with the Markforged datasheet. This investigation focuses on assessing how changes in waviness affects the compressive strength of cCFRP.

Therefore, in this study, we used a short carbon fiber/PA-6 composite material (sCFRP) to print the surface layers. Onyx® filament, produced by Markforged Inc., was employed to investigate the effect of the surface layer on compressive strength. We also experimentally investigated the effect of the surface layer on the initial fiber waviness of the continuous fibers.

2. Experimental methods

Mark Two®, produced by Markforged Inc., was used to manufacture the specimens for the cCFRP compression tests in this study. The slicing software Eiger® was used to create print paths of the specimens. The filaments used were cCFRP (cCF/PA-6: carbon fiber, Markforged Inc.) and sCFRP (sCF/PA-6: Onyx®, Markforged Inc.).

In this study, unlike the previous report [15], we measured the compressive strength in the fiber direction of a unidirectional cCFRP specimen that has the lower surface (floor), lateral surface (wall), and upper surface (roof) made of sCFRP filament. Two types of specimens, type A and type B, similar to those in the previous report, were prepared using the Mark Two 3D printer. Figure 1 shows the configuration of the specimens. The specimen width is larger than that of the specimen in the previous report [15] because it includes a wall path of sCFRP. The length of the specimen $L = 78$ mm, the width $W = 12.7$ mm, and the thickness $t = 2$ mm. One path of the wall was placed in both type A and B test specimens, and three layers each were placed for the floor and the roof. The center parts printed using the cCFRP filament were set the same as in the previous report [15]. However, the plate thickness increased by *0.4* mm due to the printing of the floor and roof, but it is expressed as *2* mm in this study.

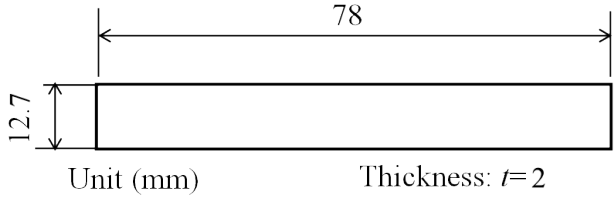

Fig. 1 Compression test specimen configuration.

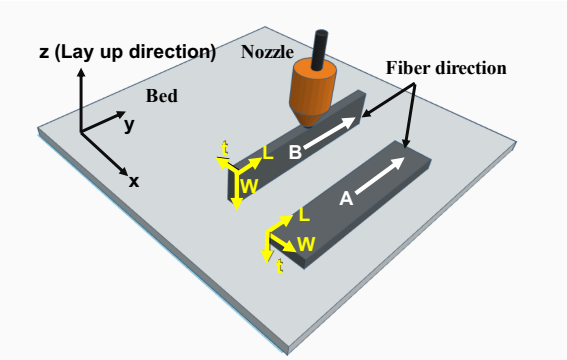

Fig. 2 Printing orientations of type A and type B specimens.

Figure 2 shows the printing orientation of the two types of specimens, A and B, fabricated using a 3D printer. In type A, a flat specimen was printed parallel to the printing bed, making the thickness direction the layup direction during printing. In contrast, for type B, the layup direction is in the width direction of the specimen. In Figure 2, *L*, *W*, and *t* represent the longitudinal, width, and thickness directions, respectively, in the specimen coordinate system. In both types of specimens, the direction of the continuous fibers is set in the longitudinal direction (*L*) of the specimen.

As mentioned earlier, sCFRP filament was used to print the wall, floor, and roof of the test specimens in this study. Figure 3 shows the printing path for type A. Folded continuous fibers are observed at the end of the cCFRP filament specimen. If a compressive load is applied from the end of the specimen, it will be applied to these folded continuous fibers. For this reason, the length in the *L* direction was *90* mm during fabrication, and after fabrication, both ends of the specimen were cut to a length of *78* mm for the compressive tests. To print a *2* mm-thick specimen, *16* layers of cCFRP were laminated in the thickness direction, and 13 paths were printed in the width direction.

Figure 4 shows the printing path of the Type B specimen. When printing a single flat specimen, the contact area with the printing bed is smaller than that corresponding to type A. Additionally, as the nozzle is higher from the printing bed, its movement tends to cause the specimen to fall over during the printing process. To address this, we fabricated two type B specimens by printing a pipe with a rectangular cross-section and cutting it after the printing process. This reduced the risk of falling over during printing. For the type B, *96* layers were laminated in the width direction of the specimen. Two paths were placed on the wall, one on the front and one on the back side, creating a test piece with a thickness of *2* mm. After printing, a woven glass fiber-reinforced epoxy (GFRP) composite material with a length of *35* mm, width of *12.7* mm, and thickness of *2.5* mm was glued as tabs, as shown in Figure 5.

The compression tests were conducted using a universal testing machine (AG-I 100kN, Shimadzu Corp.). The compression speed is 0.5 mm/min. To measure the elastic modulus, two strain gauges were attached to the center of the back and front surfaces of the specimen. Figure 6 shows the setup used for compression testing. A jig compliant with ASTM D695 was used for the testing.

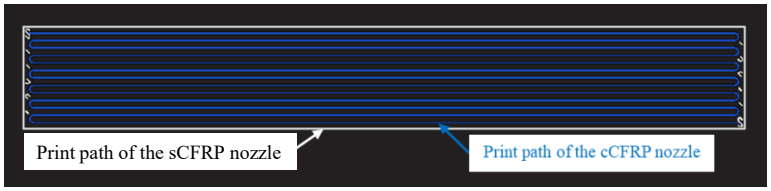

Fig. 3 Printing path of the type A specimen.

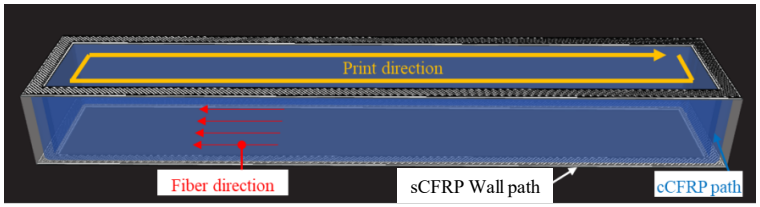

Fig. 4 Printing path of the type B specimen.

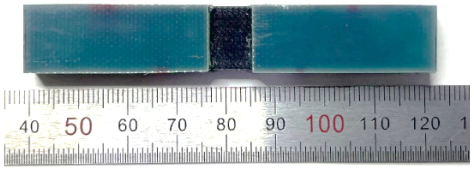

Fig. 5 Compression test specimen with GFRP tabs.

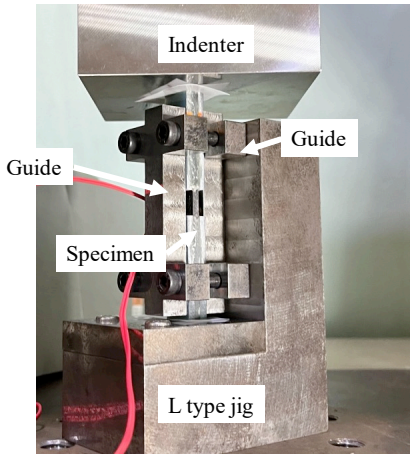

Fig. 6 Compression test setup.

The specimens used in this study were made from two materials with different mechanical properties. The compressive strain of a specimen can be measured using an attached strain gauge. However, to determine the compressive stress applied to cCFRP, in addition to the inner cCFRP layer, sCFRP is used for the wall layer with fibers aligned in the loading direction, and the floor and roof layers are aligned at ±*45*°. It is necessary to calculate this by applying the rule of mixtures to the three types of materials, including sCFRP. In type A, the wall surrounds the specimen, and the floor and roof are printed on the *L*–*W* surface using the specimen coordinates shown in Figure 2. In contrast, in type B, the floor and roof are only in the *L*–*T* plane, and the *L*–*W* plane of the specimen surface becomes the wall.

Kubota et al. [18] experimentally obtained the elastic modulus of sCFRP in each direction. Volume content can be measured on Slice software's Eiger®. Table 1 specifies the volume content determined and the elastic modulus of sCFRP. As the elastic modulus of sCFRP is smaller than that of cCFRP (*53* GPa [17]) and the volume fraction of the surfaces such as the floor, roof and wall paths is very small compared to the volume fraction of cCFRP, the rule of mixtures for a composite material composed of the three types of materials is adopted as shown in Equation (1) for simplicity.

$$\sigma_T = V_{sCFRP45}\sigma_{sCFRP45} + V_{sCFRP0}\sigma_{sCFRP0} + V_{cCFRP}\sigma_{cCFRP} \quad (1)$$

Here, $V_{sCFRP45}$ is the volume fraction of ±*45*° layer sCFRP, V_{sCFRP0} is the volume fraction of sCFRP whose printing path direction is in the *L* direction of the specimen, V_{cCFRP} is the volume fraction of cCFRP, and σ_T is the averaged stress of the specimen in the *L* direction. The compressive stress $\sigma_{sCFRP45}$ is the compressive stress of ±*45*° layered sCFRP, σ_{sCFRP0} is

the compressive stress of sCFRP with the printing path direction in the L direction of the specimen, and σ_{cCFRP} is the compressive stress of cCFRP. The following Equation (2) holds from the elastic modulus and strain ε.

$$\sigma_T = V_{sCFRP45}E_{sCFRP45}\varepsilon + V_{sCFRP0}E_{sCFRP0}\varepsilon + V_{cCFRP}\sigma_{cCFRP} \quad (2)$$

Here, ε is the specimen strain measured from the strain gauge, $E_{sCFRP45}$ is the elastic modulus of sCFRP printed in the in-plane direction, and E_{sCFRP0} is the elastic modulus of sCFRP printed in the L direction of the specimen.

Table 1 Fiber volume fraction and mechanical properties to calculate compressive stress of cCFRP.

	Type A	Type B
$V_{sCFRP45}$	*0.234*	*0.042*
V_{sCFRP0}	*0.063*	*0.281*
V_{cCFRP}	*0.703*	*0.677*
$E_{sCFRP45}$ [18]	*0.74* [GPa]	
E_{sCFRP0} [18]	*2.64* [GPa]	

3. Results and discussion

3.1 Compression test results

A compressive stress–strain diagram of the measured type A specimen is shown in Figure 7. Stress represents the stress applied to the inner-layer cCFRP and is calculated using Equation (2). In Figure 7, the strains measured from the strain gauges on both sides of the specimen are shown separately as dashed and solid lines for the five specimens. As shown in the figure, both the solid and dashed curves are almost straight lines; however, there is a slight separation in the strain

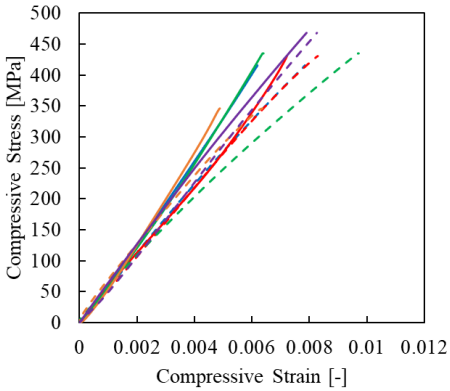

Fig. 7 Compressive stress–strain curves of type A specimens.

owing to the bending of the specimen. However, a sudden change in the strain on the front and back surfaces due to buckling just before fracture was not observed. The average compressive strength of the type A specimen was *420* MPa, and the standard deviation of the compressive strength was *44.4* MPa. This strength value is higher than the previous report of *347* MPa [15] without the sCFRP (Onyx®) layer and is consistent with the value in the Markforged datasheet [16].

Figure 8 shows the compressive stress-strain diagram of the measured type B specimens. Similar to the type A specimen, both the solid and dashed curves are almost straight lines, and there is no sudden change due to buckling until failure. Figure 9 shows a comparison between a typical example of the previous report's results [15] without a surface

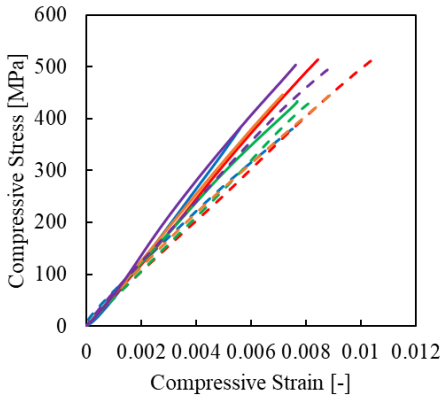

Fig. 8 Compressive stress–strain curves of type B specimen.

sCFRP layer and a typical example of the type B with an sCFRP layer in this study. As shown in Figure 9, when the sCFRP layer is present, the strain deviation on both sides of the specimen is smaller. The average compressive strength of type B specimen in this experiment was *456* MPa (standard deviation *54.8*). This variation matches the value of the Markforged datasheet [16]. The data scattering in Fig 7 and 8 comes from the specimen fabrication. It is difficult to fabricate unidirectional carbon fiber composites without fiber tension. This causes scattering of initial fiber waviness.

Table 2 shows the measured compressive strength and elastic modulus of each specimen compared with the previous results without the sCFRP layer [15]. The *t*-test was performed on the results of type A and type B with sCFRP layer, and no significant difference was noted in both the averaged strength and elastic modulus between the two specimen types. However, a significant difference was found when comparing the results with and without the sCFRP layer.

3.2 Observation results

Figures 10 and 11 present the observation results of the specimens after the compression test. It can be seen that kink-band failure has occurred, and the kink band is progressing in the layup direction in both types A and B. This is consistent with the previous results without the sCFRP layer [15] and is thought to be due to the weak lamination strength by the 3D printing process [13].

Figures 12 and 13 show the results of X-ray computed tomography (CT) observations of the cross-sections of type A and type B specimens before compression testing, respectively. The images were obtained using an X-ray CT imaging device (ScaXmate-L080H; Comscantecno Co., Ltd.). Table 3 enumerates the CT scan parameters.

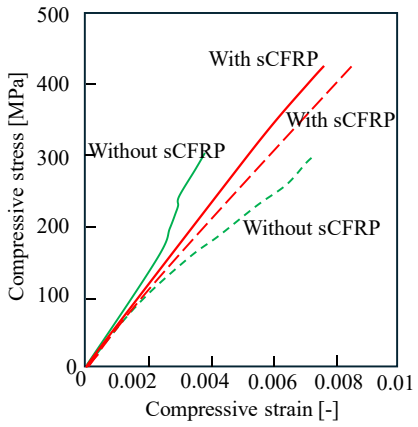

Fig. 9 Comparison between compressive stress–strain curves of type B specimen without sCFRP and that with sCFRP.

Table 2 Measured compressive strength and elastic modulus. Numbers in parentheses indicate the standard deviation.

	Without sCFRP (Onyx®) [15]		With sCFRP (Onyx®)	
	Strength [MPa] (STD)	Modulus [GPa] (STD)	Strength [MPa] (STD)	Modulus [GPa] (STD)
Type A	*347*(*37.2*)	*53.3*(*2.1*)	*420* (*44.4*)	*58.9* (*3.6*)
Type B	*323*(*28.4*)	*52.3*(*4.6*)	*456* (*54.8*)	*59.0* (*4.1*)

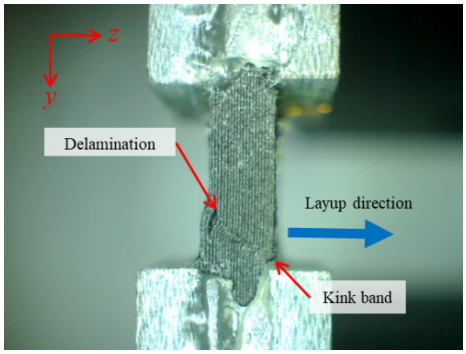

Fig. 10 Compressive failure configurations of type A specimen printed with sCFRP.

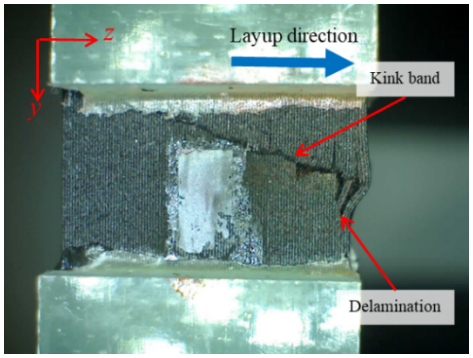

Fig. 11 Compressive failure configurations of type B specimens printed with sCFRP.

Table 3. Parameters of X-ray CT scan (ScaXmate-L080H).

Parameters	Value
X-ray tube voltage [kV]	*78*
X-ray tube current [μA]	*26*
Resolution [μm/pixel]	*19.757*
Number of projections	*1500*
Black value	*-4.8*
White value	*42.0*

Figure 12 (b) shows that the almost exact rectangular cross section is maintained by the sCFRP layer on the surface. The cCFRP was printed in two paths close to each other, and the two paths formed one set with a gap between each set. In the absence of the sCFRP layer on the surface of Figure 12 (a), the rectangular cross-section is distorted. Although pairs of printing paths are recognized, there are many gaps in the entire cross-sectional view.

In type B of Figure 13, it can be seen that in case (a) without sCFRP, the surface exhibits severe unevenness. Additionally, gaps are observed between the laminated layers, indicating extremely weak bonding between the layers. Many gaps are also present between the paths. In case (b), which uses sCFRP, the gaps between paths are smaller than those in case (a). This suggests that the use of sCFRP stabilizes the paths of cCFRP during printing, reducing surface irregularities and gaps between paths.

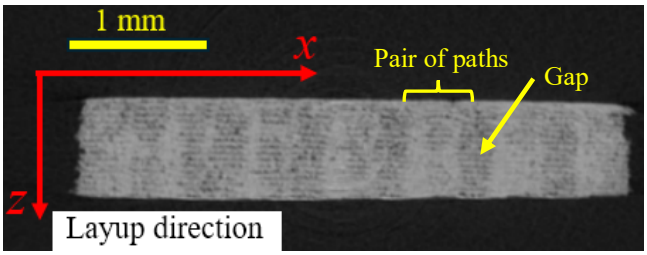

(a) Without sCFRP

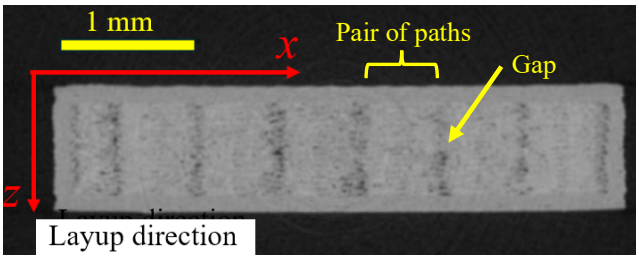

(b) With sCFRP

Fig. 12. Observations of the cross-section of the type A specimens.

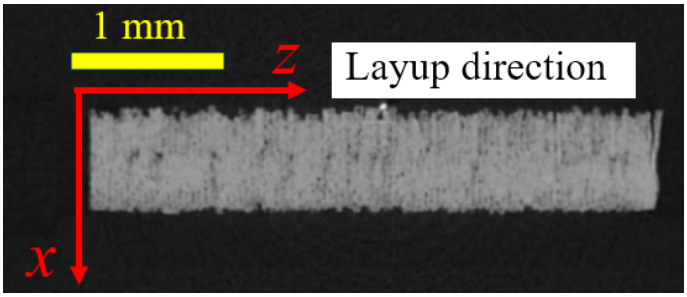

(a) Without sCFRP

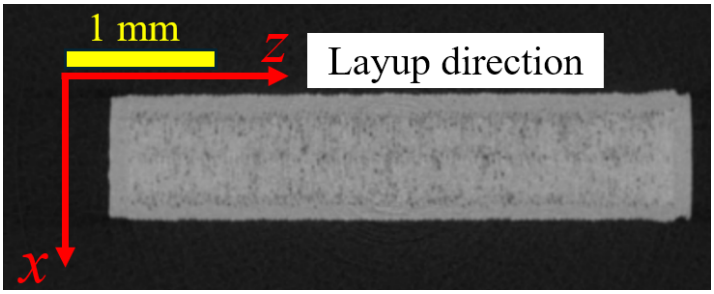

(b) With sCFRP

Fig. 13 Observations of the cross-section of the type B specimens.

The elastic modulus in Table 2 is almost equivalent to the elastic modulus of *62* GPa reported by Markforged [16] when using sCFRP. This indicates that the low strength and low elastic modulus observed when sCFRP is not used are due to the effect of voids caused by the gaps. Additionally, the difference in strain behavior of type B between the front and back sides without sCFRP (Figure 9) is likely ascribable to the difference in unevenness between the front and back sides as shown in Figure 13(a). This unevenness appears to be caused by bending deformation, possibly due to positional errors in the path of the continuous fibers and the difference in the elastic modulus of the outermost layer on the front and back sides.

Budiansky [14] demonstrated the importance of initial waviness in the axial compressive strength of cCFRP. Takahashi et al. [8] showed in finite element simulations that the average waviness of a cluster of unidirectional carbon fibers is essential, and the effect of the maximum deflection on compressive strength is small. Unfortunately, the resolution of the X-ray CT used in this study does not allow us to measure the exact waviness of individual carbon fibers. Therefore, we measured the maximum measurable waviness of the X-ray CT scanner used in this study and qualitatively evaluated the initial waviness. We hypothesize that the maximum fiber waviness is positively correlated with the average fiber waviness in this study. Figures 14 (a)–(d) show the measurement results of maximum waviness with and without sCFRP in types A and B. Table 4 specifies the maximum measured waviness values.

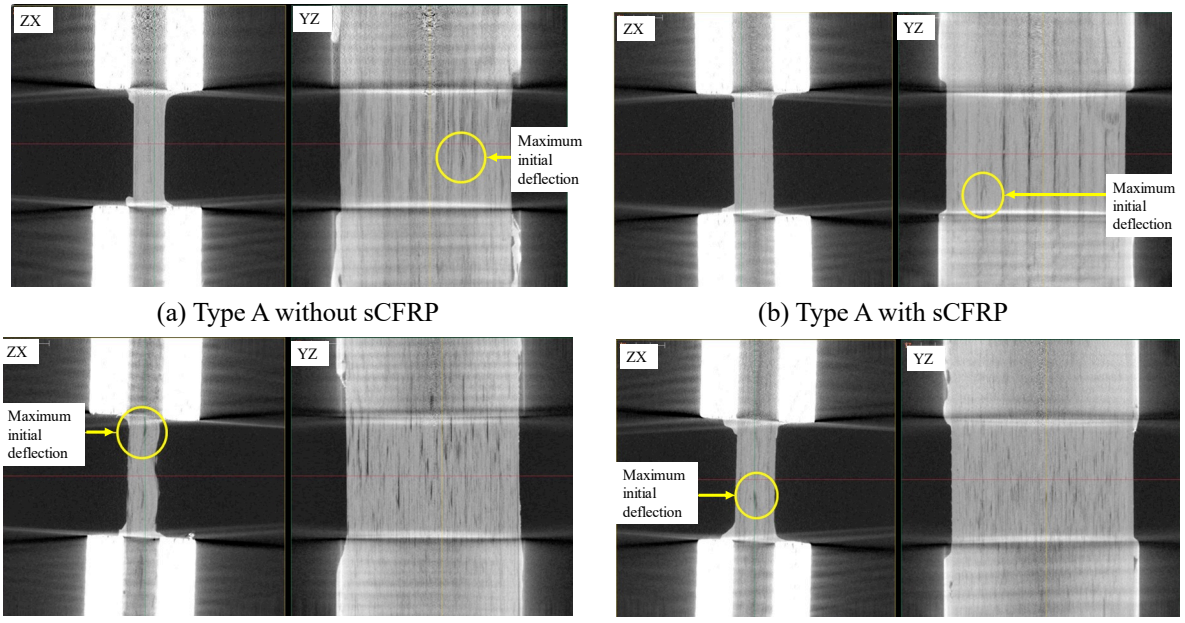

(a) Type A without sCFRP (b) Type A with sCFRP

(c)Type B without sCFRP (d) Type B with sCFRP

Fig. 14 Measurements of the maximum initial waviness of carbon fibers using X-ray CT.

Table 4 Angle of the waviness of the most prominently undulated cCFRP paths.

Specimen type	Angle of waviness [deg]	Compressive strength [MPa]
Type A without sCFRP	*13.8*	*347*
Type A with sCFRP	*6.07*	*420*
Type B without sCFRP	*9.99*	*323*
Type B with sCFRP	*4.48*	*456*

From the results in Table 4, it can be seen that using sCFRP in both types A and B suppresses waviness by about half. Additionally, type B without sCFRP, which has the lowest compressive strength, exhibits the highest waviness. Conversely, the case with type B with sCFRP, which has the highest compressive strength, shows the lowest waviness. While this maximum waviness value does not directly provide the compressive strength, it qualitatively represents the magnitude of the compressive strength. Therefore, by printing sCFRP walls, floors, and roofs, the paths of cCFRP are able to suppress waviness and improve compressive strength.

4. Conclusions

In this study, 3D-printed cCFRP was fabricated using two different orientations, and the effect of walls, floors, and roofs printed by sCFRP on the compressive properties was investigated. Cross-sectional observations were performed using X-ray CT to identify the cause of the decrease in compressive strength. The following conclusions were obtained:

(1) Creating a surface with sCFRP on 3D-printed cCFRP improves the compressive strength and compressive elastic modulus.

(2) The kink band during compression failure of 3D-printed cCFRP always evolves in the layup direction.

(3) Printing sCFRP walls, floors, and roofs makes it difficult for cCFRP paths to move, suppresses waviness, and improves compressive strength.

References

[1] Hsiao H.M, Daniel I.M. Effect of fiber waviness on stiffness and strength reduction of unidirectional composites under compressive loading. Composites Science and Technology 1996;56:581–593.

[2] Soutis C, Curtis P.T. A method for predicting the fracture toughness of CFRP laminates failing by fibre microbuckling. Composites Part A 2000;31:733-740.

[3] Yokozeki T, Ogasawara T, Ishikawa T. Nonlinear behavior and compressive strength of unidirectional and multidirectional carbon fiber composite laminates. Composites Part A 2006;37(11):2069–2079.

[4] Jumahat A, Soutis C, Jones F.R, Hodzic A. Fracture mechanisms and failure analysis of carbon fibre/toughened epoxy composites subjected to compressive loading. Composite Structures 2010;92:295–305.

[5] Ueda M, Mimura K, Jeong T-K. In situ observation of kink-band formation in a unidirectional carbon fiber reinforced plastic by X-ray computed tomography imaging. Advanced Composite Material 2016;25(1):31–43.

[6] Ueda M, Tasaki Y, Kawamura C, Nishida K, Honda M, Hattori K, Miyanaga T, Sugiyama T. Estimation of axial compressive strength of unidirectional carbon fiber reinforced plastic considering local fiber kinking. Composites Part C 2021;6:100180.

[7] B. Budiansky. Micromechanics, Computers & Structures 1983;16:3-12.

[8] Takahashi T, Ueda M, Miyoshi K, Todoroki A. Initiation and propagation of fiber kinking from fiber undulation in a unidirectional carbon fiber reinforced plastic. Composites Part C 2020:100056.

[9] https://i-maker.jp/blog/mark-one-1641.html (2014), (Access 6 May 2024)

[10] Matsuzaki R, Ueda M, Namiki M, Jeong T.K, Asahara H, Horiguchi K, Nakamura T, Todoroki A, Hirano Y. Three-dimensional printing of continuous-fiber composites by in-nozzle impregnation, Scientific Reports 2016;6:23058.

[11] Van Der Klift F, Koga Y, Todoroki A, Ueda M, Hirano Y, Matsuzaki R. 3D printing of continuous carbon fibre reinforced thermo-plastic (CFRTP) tensile test specimens. Open Journal of Composite Materials 2016;6(1):18-27.

[12] Blok L.G, Longana M.L, Yu H, Woods B.K.S. An investigation into 3D printing of fibre reinforced thermoplastic composites. Additive manufacturing 2018;22:176-186.

[13] Todoroki A, Oasada T, Mizutani Y, Suzuki Y, Ueda M, Matsuzaki R, Hirano Y. Tensile property evaluations of 3D printed continuous carbon fiber reinforced thermoplastic composites. Advanced Composite Materials 2020;29(2):147-162.
[14] Iragi M, Pascual-González C, Esnaola A, Lopes C.S, Aretxabaleta L. Ply and interlaminar behaviors of 3D printed continuous carbon fibre-reinforced thermoplastic laminates; effect of processing conditions and microstructure. Additive Manufacturing 2019;20:100884.
[15] Bin Zakaria A. Z, Takahashi T, Todoroki A, Ueda M. Kink band orientation of 3D printed continuous carbon fiber composites under compressive loading. Advanced Composite Materials 2024;33(2):250-268.
[16] https://s3.amazonaws.com/mf.product.doc.images/Datasheets/Translations/JA/Markforged_CompositesV5_ja.pdf
[17] Ahmad Zuhair bin Zakaria, Takuya Takahashi, Akira Todoroki, Masahito Ueda, Kink band orientation of 3D printed continuous carbon fiber composites under compressive loading. Advanced Composite Materials 2024;33(2):250-268.
[18] Kubota M, Hayakawa K, Todoroki A. Effect of build-up orientations and process parameters on the tensile strength of 3D printed short carbon fiber/PA-6 composites. Advanced Composite Materials 2022;31(2):119-136.